THE UNIVERSITY OF RHODE ISLAND

University of Rhode Island
DigitalCommons@URI

Chemistry Faculty Publications

Chemistry

11-13-2017

Conductance-Based Profiling of Nanopores: Accommodating Fabrication Irregularities

Y. M. D. Y. Bandara
University of Rhode Island

Maher Harb
University of Rhode Island

Jonathan W. Nichols
University of Rhode Island

Buddini Iroshika Karawdeniya
University of Rhode Island

Jason R. Dwyer
University of Rhode Island, jason_dwyer@uri.edu

Follow this and additional works at: https://digitalcommons.uri.edu/chm_facpubs

Citation/Publisher Attribution

Bandara, Y. M. N. D. Y., Nichols, J. W., Karawdeniya, B. I., & Dwyer, J. R. (2017). Conductance-Based Profiling of Nanopores: Accommodating Fabrication Irregularities. *Electrophoresis*, *39*, 626-634. doi: 10.1002/elps.201700299
Available at: http://dx.doi.org/10.1002/elps.201700299

This Article is brought to you by the University of Rhode Island. It has been accepted for inclusion in Chemistry Faculty Publications by an authorized administrator of DigitalCommons@URI. For more information, please contact digitalcommons-group@uri.edu. For permission to reuse copyrighted content, contact the author directly.

Conductance-Based Profiling of Nanopores: Accommodating Fabrication Irregularities

The University of Rhode Island Faculty have made this article openly available. Please let us know how Open Access to this research benefits you.

This is a pre-publication author manuscript of the final, published article.

Terms of Use

This article is made available under the terms and conditions applicable towards Open Access Policy Articles, as set forth in our Terms of Use.

This article is available at DigitalCommons@URI: https://digitalcommons.uri.edu/chm_facpubs/96

Conductance-Based Profiling of Nanopores: Accommodating Fabrication Irregularities

Y.M. Nuwan D.Y. Bandara, Jonathan W. Nichols, Buddini Iroshika Karawdeniya, and Jason R. Dwyer.

Final version of manuscript available at

http://onlinelibrary.wiley.com/doi/10.1002/elps.201700299/abstract

DOI: 10.1002/elps.201700299

Supplementary information freely available at
http://binarystore.wiley.com/store/10.1002/elps.201700299/asset/supinfo/elps6375-sup-0001-SuppMat.docx?v=1&s=9e613734376b15977546f7caef2e1d06d519e0a5

Conductance-Based Profiling of Nanopores: Accommodating Fabrication Irregularities

Y.M. Nuwan D.Y. Bandara, Jonathan W. Nichols, Buddini Iroshika Karawdeniya, and Jason R. Dwyer.

Department of Chemistry, University of Rhode Island, 140 Flagg Road, Kingston, RI, 02881, United States.

E-mail: jason_dwyer@uri.edu. Phone 1-401-874-4648. Fax 1-401-874-5072.

KEYWORDS. dielectric breakdown; nanopore; nanopore conductance; nanopore defect; pore density; silicon nitride nanopore.

Abbreviations. TEM-transmission electron microscopy; STEM-scanning transmission electron microscopy; EM-electron microscopy; MPVI-multilevel pulse-voltage injection

Total Number of Words: 4880

ABSTRACT:

Solid-state nanopores are nanoscale channels through otherwise impermeable membranes. Single molecules or particles can be passed through electrolyte-filled nanopores by, e.g. electrophoresis, and then detected through the resulting physical displacement of ions within the nanopore. Nanopore size, shape, and surface chemistry must be carefully controlled, and on extremely challenging <10 nm-length scales. We previously developed a framework to characterize nanopores from the time-dependent changes in their conductance as they are being formed through solution-phase nanofabrication processes with the appeal of ease and accessibility. We revisited this simulation work, confirmed the suitability of the basic conductance equation using the results of a time-dependent experimental conductance measurement during nanopore fabrication by Yanagi *et al.*, and then deliberately relaxed the model constraints to allow for (1) the presence of defects; and (2) the formation of two small pores instead of one larger one. Our simulations demonstrated that the time-dependent conductance formalism supports the detection and characterization of defects, as well as the determination of pore number, but with implementation performance depending on the measurement context and results. In some cases, the ability to discriminate numerically between the correct and incorrect nanopore profiles was slight, but with accompanying differences in candidate nanopore dimensions that could yield to post-fabrication conductance profiling, or be used as convenient uncertainty bounds. Time-dependent nanopore conductance thus offers insight into nanopore structure and function, even in the presence of fabrication defects.

1 INTRODUCTION:

Nanopores are a rising tool for single-molecule science, featuring prominently in DNA sequencing efforts, but with broader reach into biophysics, and bioanalytical and materials chemistry.[1-12] The nanopore heart of these techniques is a nanofluidic channel generally less than 100 nm in all dimensions, formed through a membrane or support, with the particular dimensions dictated by the analyte and method. The essential determinants of nanopore performance include the elements of three general nanopore-specific parameter groupings: nanopore size, shape, and surface chemistry.[13-19] Even the most basic nanopore operating configuration illustrates the importance of these parameters, and also provides a means for assaying them. A nanopore is positioned as the sole fluid path between two wells of electrolyte solution. Application of suitable voltages, typically ≤200 mV, across the impermeable support membrane drives ion passage through the nanopore. The resulting open-pore ionic conductance, G, is determined by the bulk solution conductivity, K, by the size and shape of the nanopore (here captured in volume and surface integrals, $A = \left(\int \frac{dz}{\pi(r(z))^2}\right)^{-1}$ and $B = \left(\int \frac{dz}{2\pi r(z)}\right)^{-1}$, respectively), and by properties of the nanopore-solution interface[13, 16, 18, 20-23]

$$G = K \cdot A(r, L) + \mu|\sigma| \cdot B(r, L) = G_{\text{bulk}} + G_{\text{surface}} \quad (1)$$

where σ is the nanopore surface charge density that attract counterions of mobility, μ. The pore has a radius, *r(z)* , that can vary along length, L, of the pore (aligned with the z-axis as shown in Figure S1). More complex theoretical approaches exist—a formulation including the access resistance term (neglected here for simplicity) is discussed in the supporting information (see Equation S1, Figure S2 and associated discussion)—but this straightforward conductance model provides a tractable and useful framework with good agreement with the measured conductance

of nanopores across a range of experimentally determined sizes and shapes.[13, 16, 18, 20, 21, 24] As a species of interest passes through the nanopore, or is entrained therein, it perturbs the open-pore flow of ions, and frequently generates an analyte-specific current blockage (or enhancement)[4, 10, 13, 17, 23]. A simple analytical model for the conductance blockage wrought by the extension of an analyte such as DNA, of radius r_{analyte}, through the length of a uniformly cylindrical nanopore of radius r_0, illustrates more directly the importance of nanopore dimensions:

$$\chi_B \equiv \frac{(\langle G\rangle - \langle G_b\rangle)}{\langle G\rangle} \cong \left(\frac{r_{\text{analyte}}}{r_0}\right)^2 \quad (2)$$

with $\langle G\rangle$ and $\langle G_b\rangle$ the time-averaged conductances of open, and analyte-filled, nanopore.[25] The more complex set of phenomena and parameters underpinning the current blockage explains the experimentally demonstrated ability to extract meaningful molecular information, such as detecting nucleotide sequence in such a strand of DNA.[2, 4, 8, 10, 17, 19, 26, 27] The details of nanopore surface charges are not only important in the context of conductance as in Equation 1, but extend to augmenting electrophoretic control over analyte motion through the nanopore with electroosmosis, and to allowing nanopores to analyte-select not only based on size, but also by charge.[9, 28-31] Conductance-based nanopore characterization is, in fact, uniquely positioned to provide geometric and chemical insights into nanopore properties. It is also exceedingly important in the context of solution-phase nanopore fabrication methods where post-fabrication microscopic characterizations are undesirable. The prevailing approach has been to assume formation of a single nanopore when one is intended, and to overlook possible structural defects. Inaccurate nanopore models will affect the quality of conductance characterizations, and other work has shown (and taken advantage of) the influence of internal nanopore structural irregularities on analyte current blockages.[32] While it is essential to control the size of isolated nanopores for

single-molecule characterization and sensing applications; the use of arrays of nanopores as filters for physical and chemical separations multiplies the challenges and underscores the need to detail the formation of even single nanochannels.[11]

The extreme, ~10 nm feature size has historically been challenging to nanopore fabrication (and characterization) efforts. Methods have tended to be instrumentation-intensive, using charged-particle microscopes such as scanning and (scanning) transmission electron microscopes (SEM and (S)TEM), and helium ion microscopes, or ion accelerator facilities to prepare membranes for subsequent chemical etching steps.[33-37] More recently, ~20 V potentials applied across thin membranes immersed in electrolytes conventionally used for nanopore experiments resulted in (controlled) dielectric breakdown of the films, and could produce size-tuned nanopores following voltage-assisted etching.[38] This truly low-overhead approach can yield <10 nm diameter nanopores, and produces them reliably wetted for use, without the risks of drying and surface contamination from steps such as TEM-based fabrication (or examination). A similarly all-solution-based approach uses deposition of largely conformal films to shrink suitable pores to the desired final dimension.[9, 39] By deliberately and beneficially removing high-magnification charged-particle microscopes from the fabrication workflow, however, the opportunity to immediately image the fabricated pores is lost. We therefore explored existing nanopore conductance formalisms[13, 18] and developed a framework to use conductance to characterize nanopore size, shape, and surface chemistry.[14-16] We most recently showed that the method could yield real-time insight into these nanopore properties during solution-phase fabrication processes such as those outlined above.[14] In all instances, however, the simulations assumed perfectly formed single nanopores. Here we (1) deliberately introduce defects into the pore models, and we moreover (2) allow for the possibility that a measured conductance arises from two separate

nanopores forming in the same membrane (denoted a double pore). The latter allowance arises from TEM observations, post-pore fabrication, showing that dielectric breakdown formation of nanopores using unoptimized multilevel pulse-voltage injection could yield more than one pore.[40] Conductance-based measurements should allow for these realities, at least through the setting of reasonable uncertainty levels. We focus here on nanopores formed in thin, free-standing silicon nitride membranes, so that our numerical simulations use parameter values from the most commonly used nanopore material platform. The films are amorphous and thus not inherently prone to anisotropic etching,[41] and silicon nitride is notably resistant to structural and chemical modification absent deliberate action.

2 METHODS

The form of Equation 1 means that a single measured conductance does not yield a single unique solution for the nanopore size and shape.[14-16] One can gain more degrees of freedom by measuring the conductances at two different solution conductivities, K,[15, 16] or after (or during) controlled structural modifications.[14, 15] A time-dependent framework was developed and examined conventionally in earlier work—without considering either defects or multiple pores.[14] During nanopore formation—by dissolution or deposition of material—the nanopore conductance is a function of time because the dimensions of the nanopore, $\{q_j(z,t)\}$, are changing in time, t:

$$\frac{dG}{dt} = K\sum_j\left(\frac{\partial A}{\partial q_j}\right)\frac{dq_j}{dt} + \mu|\sigma|\sum_j\left(\frac{\partial B}{\partial q_j}\right)\frac{dq_j}{dt}. \quad (3)$$

This particular implementation can determine geometries with two free parameters, and we chose the limiting (minimum) radius, $r_0(z,t)$, and the total nanopore length, $L(t)$.[14] The presence of a defect disrupts the usual cylindrical symmetry. For a membrane with more than one nanopore,

the nanopores are conductors in parallel (with identical surface chemistries and electrolyte contents) so that their conductances would be added directly, $G = \sum_n G_n$. Using a single measurement of the conductance at a single time t_i, it is not possible to distinguish between a single large pore and two smaller pores, or between a pore with or without a defect, when $G(t_\mathrm{i}, \{q_j(t_\mathrm{i})\}) = G(t_\mathrm{i}, \{q'_j(t_\mathrm{i})\})$.[14] The size- and geometry-dependence of the conductance change in time, however,

$$\frac{dG}{dt} = \sum_n \left(K \sum_j \left(\frac{\partial A_n}{\partial q_j} \right) \frac{dq_j}{dt} + \mu |\sigma| \sum_j \left(\frac{\partial B_n}{\partial q_j} \right) \frac{dq_j}{dt} \right) \tag{4}$$

provides a much-needed degree of freedom to possibly differentiate between such configurations. The characterization method then has a very simple implementation: measurements of several sequential experimental conductance values at times $\{t_i, \ldots\}$, $\{G(t_i, \{q_j(t_i)\}), \ldots\}$, are the inputs to the geometry optimization of candidate nanopore profiles. We simulated the experimental conductances using the experimentally supported Equation 1 in conjunction with experimentally supported nanopore profiles, and then fit the data using candidate nanopore profiles.[16, 18] The focus was whether including either defects or double pores would negatively affect the feasibility of the approach augured by the formalism. To allow this emphasis, the effect of measurement noise on the conductance was neglected. The change in nanopore radius in time, $\frac{dr}{dt} = v_\mathrm{mt}$, occupies a privileged role as the material transfer rate (with opposite signs for etching and deposition). We used a constant $|v_\mathrm{mt}| = 0.6\,\mathrm{nm/h}$ to highlight the nonlinear dependence of conductance on geometry in Equations 1, 3, and 4, and in keeping with the linear etch rates common to micromachining, but the method does not depend on that particular magnitude or time-dependence.[14, 41] We chose four nanopore profiles finding widespread use: cylindrical, double-conical, conical-cylindrical, and hyperbolic (Figure S1), but the method does not hinge on these

particular choices.[13, 16, 18, 37, 42] The label r_0 is used here to denote the radius of the cylindrical pores, and the minimum radius (at any given time) of the pores with radii varying with z; "pinch" and "outline" labels will be introduced for the r_0 of cylindrical nanopores with defects. All profiles were conventionally restricted to two free parameters, each, (r_0 and L) with the outer radius of the three tapered profiles fixed to be 10 nm greater than their corresponding r_0, and the initial length of the inner cylinder of the conical-cylindrical pore restricted to 0.6 times its overall length, $L(t_0)$, where t_0 is the starting time. To model the double pore case, the two pores were set to be identical. Parameter values and calculations were consistent with previous work:[14-16, 22] 1 M potassium chloride electrolyte solution in water, K=14.95 $S \cdot m^{-1}$, pH 7.0, and silicon nitride surface pK_a=7.9, with σ calculated in the usual way.[16, 22] The influence of solution pH is outlined in Figure S3 and the discussion immediately preceding it. For the defect-free pores, surface-deposited films were treated in a piecewise curved manner to maintain a uniform surface coating thickness (Figure S1) across the entire nanopore surface.[14] For the case of the pores with defects (Figure 1a) the half-cylinder protrusions running along the full length of the pore interior were centered on the pore outline, opposite each other. Simulations of $G(t_i)$ were performed using 0.01 nm step sizes in the nanopore radius (or 1 minute increments given v_{mt}), and fits to $r_0(t_0)$ versus t were plotted using 0.05 nm increments.

3 RESULTS AND DISCUSSION:

Post-fabrication comparisons of electron microscopic and steady-state conductance measurements support the independent use of Equation 1 for nanopore characterization.[13, 16, 18, 20, 21, 24] Conductance measurements recorded during a fabrication process such as dielectric breakdown, however, occur in a different context than post-fabrication measurements.[38, 43] In Figure 2, we used experimental multilevel pulse-voltage injection (MPVI) nanopore formation

measurements—both steady-state and time-dependent—by Yanagi *et al.*[43] to test whether a formalism such as Equation 1 would yield reasonable real-time size determinations using the time-dependent conductance of a forming nanopore. Yanagi *et al.*[43] measured the steady-state conductances, G, of post-fabrication pores and then used TEM imaging to determine their mean r_0. With appropriate consideration of the usual caveats of EM nanopore characterization[14, 16], along with possible consequences of nanopore dewetting and handling, post-fabrication electron microscopy provides a valuable, albeit instrumentation- and expertise-intensive, measure of nanopore size. Unsurprisingly, we obtained good fits to post-fabrication data using Equation 1 (Figure 2a)—in particular with a conical-cylindrical profile with conventional constraints (see above)—and using Equation S1 (Equation 1 with an access resistance term—see discussion below) with cylindrical models with effective or adjustable fitting parameters. To correlate Yanagi *et al.*'s[43] measured G and mean r_0 without biasing the fit with an explicit choice of nanopore shape, we modified the cylindrical model of Equation S1 by replacing G_{bulk} with αG_{bulk}, and G_{surface} with βG_{surface}. We optimized the parameters α and β using the fit to the experimental data (with known r_0, L, and G) in Figure 2a to correlate experimental post-fabrication nanopore conductances and mean nanopore radii by TEM, $r_{0,\text{TEM}}^{\alpha,\beta}(G)$. We then used $r_{0,\text{TEM}}^{\alpha,\beta}(G)$ to convert Yanagi *et al.*'s[43] time-dependent measurements of the conductance into nanopore size as a function of time, $r_{0,\text{TEM}}^{\alpha,\beta}(t_i)$ (Figure 2b). In this context, the function $r_{0,\text{TEM}}^{\alpha,\beta}(G)$ is thus better thought of as simply a fit function relating nanopore conductance and TEM-based size, rather than representing a particular model choice for the nanopore conductance. Finally, for each $G(t_i)$ data point of Figure 2b, we calculated $r_{0,\text{candidate}}(t_i)$, with all other parameters fixed, for each of the candidate nanopore profiles, and compared the results with $r_{0,\text{TEM}}^{\alpha,\beta}(G)$ (Figure 2c). The experimental $G(t_i)$ of Yanagi *et al.*[43] was fit best, using Equation 1, by a conical-cylindrical model with overall length equal

to the nominal membrane thickness. The cylindrical model using Equation S1 and with an effective length equal to a fraction of the nominal membrane thickness[43] did not fit as well as the conical-cylindrical model, but outperformed the remaining candidates. Overall, Equations 1 and S1 produce reasonable nanopore sizes when applied to conductance data recorded during nanopore fabrication. As discussed in earlier work[14], a time-dependent material-transfer rate, $\nu_{\mathrm{mt}}(t)$, is no impediment to the time-dependent conductance profiling framework.[14]

As the first application of Equation 1 to more complex nanopore configurations, we investigated the effect of defects on our ability to extract reasonable geometric descriptions of nanopore sizes. Figure 1a shows a top-down view of defects in cylindrical nanopores ($L(t_0) = 10\,\mathrm{nm}$). Figure 1a also shows one of the key challenges of conductance-based nanopore characterizations: all of the different profiles shown have, by Equation 1, the same 200 nS conductance. With larger initial defect size, the initial radius of the cylindrical outline of the nanopore (the "outline radius", $r_0^{\mathrm{outline}}(t_0)$) must also be larger to compensate for the internal volume lost for ionic transport. Defects distort the circular symmetry of the nanopore and introduce "pinch points" (as illustrated in Figure 3, characterized by the radius of a cylinder just fitting between the two protrusions—the "pinch radius", $r_0^{\mathrm{pinch}}(t_0)$) that could preclude analyte passage where a defect-free pore of equivalent conductance could allow passage. Such a failure, of course, is diagnostic, but would require the addition of gauging molecules or particles (compatible with the fabrication conditions) if it were to be used for real-time monitoring of the fabrication. Such adjuncts could naturally be used post-fabrication.[44, 45] Figure 1b shows the evolution of a cylindrical nanopore with 1 nm-radius defects: as more material is added to the surface with time, the nanopore interior becomes increasingly anisotropic. Depending on defect size, shape, and position, depositing material onto the surface of a pore with defects could readily lead to

overlapping Debye layers followed by physical scission of a single pore into two distinct pores. The comparison of single and double pore systems thus also overlaps with the consideration of fabrication defects. Figure 1c illustrates the heart of the method motivated by the form of Equations 1 and 3: it shows the time evolution, with identical material transfer rates, of the nanopore profiles shown in Figure 1a. For small nanopore sizes where Debye layers overlap, more sophisticated treatments than Equation 1 are required, but as a guide to the eye we plotted the conductance until $r_0^{\text{pinch}} = 0$.[15, 46] From their identical initial value, the conductances of the different profiles differentiate in time, in spite of the constant material transfer rate changing all outline and pinch radii at the same rate.

When nanopore dimensions are changed during fabrication, the change in conductance with time is measured without knowledge of the presence or absence of defects. The question is whether the time-trace of the conductance can reveal the presence of defects or not—and if not, how serious the error in the resulting nanopore characterizations might be. To explore this, we chose to simulate (abbreviated to "sim" in labels) the time-dependent conductances, $G_{\text{case}}^{\text{sim}}(t_i)$ (case denotes defect size), for two cylindrical nanopores with $G_{\text{case}}^{\text{sim}}(t_0) = 200$ nS and $r_0^{\text{pinch}}(t_0) = 4$ nm: one with two 0.1 nm-radius defects, and the other with two 1.0 nm-radius defects (and lengths $L(t_0)$ ~4.1 and ~5.9 nm, respectively, dictated by the conductance and radii). We attempted to fit these data by using the (known) material transfer rate and varying the dimensions of three candidate nanopore profiles: a defect-free cylindrical nanopore, and profiles with 0.1 and 1.0 nm-radii defects. The question was whether fitting to the $G_{\text{case}}^{\text{sim}}(t_i)$ would reveal the existence and size of defects. A step-by-step tutorial for this process is provided in earlier work,[14] which we abbreviate here to allow a suitable focus on fabrication irregularities. The initial conductance, $G_{\text{case}}^{\text{sim}}(t_0)$, was used to determine the (infinite) set of $\left\{\left(r_{0,\text{candidate}}(t_0), L_{\text{candidate}}(t_0)\right)\right\}$ for which

$G_{\text{candidate}}(t_0) = G_{\text{case}}^{\text{sim}}(t_0)$. After the dimension changes from depositing material at the known rate (outline and pinch radii diminish at ν_{mt}, whereas the cylinder length increases at $2\nu_{\text{mt}}$), only one pairing $\left(r_{0,\text{candidate}}(t_0), L_{\text{candidate}}(t_0)\right)$ for each candidate also satisfied $G_{\text{candidate}}(t_1) = G_{\text{case}}^{\text{sim}}(t_1)$. This answer gave the unique initial nanopore size for each candidate with its specified defect size, but could not be used to identify the simulated defect size. That is, all three candidate profiles could exactly reproduce the two simulated conductances. After propagating the deposition one more time from the three different $\left(r_{0,\text{candidate}}(t_0), L_{\text{candidate}}(t_0)\right)$, only one pair of initial nanopore dimensions gave $G_{\text{candidate}}(t_3) = G_{\text{case}}^{\text{sim}}(t_3)$. Figure 3 summarizes this behavior: the ordinate is the initial nanopore radius, $r_{0,\text{candidate}}(t_0)$, that, after deposition until time t_i, would give $G_{\text{candidate}}(t_i) = G_{\text{case}}^{\text{sim}}(t_i)$ (the dimensions at time t_i are readily calculated from the initial dimensions and the known material transfer rate). When the candidate profile (here, defect size) matches the simulated profile, then all the $r_{0,\text{candidate}}(t_0)$ from each t_i are equal to each other, and equal to $r_{0,\text{case}}^{\text{sim}}(t_0)$, and the line connecting the data is horizontal. When the candidate profile is incorrect, then the plotted data is no longer horizontal. Thus, in Figure 3a, when the simulated data is generated using a cylindrical pore with a 0.1 nm-radius defect, only the fit data using the 0.1 nm-defect candidate pore is perfectly horizontal. The defect-free nanopore fit data is close to horizontal and overlaps substantially with the outline radius of the simulated pore, but the 1 nm-defect fit data has a larger nonzero slope and is therefore the incorrect candidate. While $r_0^{\text{outline}}(t_0)$ of the 1 nm-defect candidate was not substantially larger than the true $r_0^{\text{outline}}(t_0)$, its small $r_0^{\text{pinch}}(t_i)$ would suggest an incorrect threshold for analyte size-exclusion. Figure 3b shows that a 1 nm-defect simulated pore is successfully fit only with a 1 nm-defect candidate pore, and that radii for the remaining two candidates lie between limits set by the pore with the larger defect. In both

fitting examples, the slopes of the fit data provide an indication of the correct defect magnitude, being positive when the candidate defect is too large, and negative when the candidate defect is too small. One might thus imagine a strategy in which a wider range of candidate defect sizes were used to more readily indicate the presence and provide bounds for the size of a defect. The feasibility of the method thus extends from the formalism to successful numerical examples, but these model calculations portend limitations in experimental implementation: $\Delta r_{0,\mathrm{candidate}}(t_0)\sim 0.1\mathrm{nm}$ for incorrect candidates, compared to the full 2 nm deposition thickness. In the presence of measurement noise, or with an unfavorable combination of defect size, ν_{mt}, fabrication time, and number of conductance measurements, for example, even detection of defects may elude real-time analysis.

We extended this exploration of the effect of defects by considering the effect of candidate nanopore shape on the conductance-based geometry optimization. Figure 4a illustrates the underlying premise. At t_0, the six listed nanopore profiles have identical 200 nS conductances and $L(t_0) = 10$ nm, generated by different $r_0(t_0)$. As material deposition narrows the nanopore constrictions at a constant linear rate (inset), all of the conductances diverge from each other in time. This occurs in spite of, for example, the r_0^{pinch} of the 1.0 nm-defect cylindrical pore and the r_0 of the conical-cylindrical pore having essentially identical values over time. Figures 4b and c use this behavior quantitatively. The same procedure used for Figure 3 was used to fit the simulated conductances of cylindrical nanopores with $r_0^{pinch}(t_0) = 5.0$ nm, and two defects of either 0.1 or 1.0 nm radius, with defect-free pores representing typical nanopore shapes. Even the smaller, 0.1 nm defects caused the defect-free cylindrical nanopore to be unable to fit the simulated conductance. The correct candidate profile—0.1 nm defects inside a cylindrical profile—gave a perfectly horizontal line when fit to the simulated 0.1 nm-defect data. Fitting with the conical-

cylindrical nanopore, however, generated nearly horizontal data, likely because the distinct narrow and wide sections of the profile (including constraints) were able to approximate the defect-bearing cylinder's balance of pinch and outline radii. The radius of the opening through the inner cylinder ($r_{0,\text{conical-cylindrical}}(t)$), however, was smaller than for the simulated profile. For the simulated cylindrical pore with the larger, 1.0 nm defect, the fitting procedure again returned the correct profile and defect size. Once again, the conical-cylindrical profile fit data was almost horizontal with the wrong radius, although lying between the pinch and outline radii of the defect model. Depending on the size, distribution, number of defects, and current noise, it may be difficult to use this conductance model to distinguish, in real-time during formation, between an ideal pore of a given shape, and a pore of a different shape, but with defects. It may be necessary to then resort to more involved post-fabrication approaches.[15, 16, 44, 45] Indeed, one may be forced to adopt a strategy of repeated cycles of incomplete fabrication—with real-time profiling—followed by more in-depth characterization. In such a case it is important to understand the inherent uncertainties—such as the error in r_0—of these real-time characterization procedures to ensure that the fabrication cycles do not pass by the desired final size.

A second complication for nanopore formation is the formation of more than one pore when only one is intended. Microscopy can be used to directly enumerate the pore number, but at the cost of instrumentation and user burdens, and possible nanopore surface contamination, among other drawbacks. We wanted to determine if conductance could provide any insight into this possible problem of multipore formation. We explored the case of double pores of matching size and shape. Figure S4 illustrates that the conductance change in time provides the prospect of differentiating between single and double pore systems, just as it did for single pores of different shapes.[14]

To explore whether the conductance time trace could reliably determine the size and number of the pores during their fabrication, we simulated conductances for single and double pore configurations of the four profiles in Figure S1, choosing 200 nS as a convenient initial conductance. Double pores for each shape were identical in size to each other. The conductance fitting in Figure 5 mirrors that of Figure 3 and 4b,c. For each column, a given profile with a single (a-d) or double (e-h) pore was chosen and used to calculate a minimum of three simulated conductance values in time: $G_{\text{case}}^{\text{sim}}(t_0)$, $G_{\text{case}}^{\text{sim}}(t_1)$, and $G_{\text{case}}^{\text{sim}}(t_2)$, with additional $G_{\text{case}}^{\text{sim}}(t_i)$ providing added robustness (case here denotes profile and pore number). The broad outlines of the results detailed in Fig. 5a-d and e-h are that one-pore simulated conductances were fit by the one-pore candidate profiles of the correct shape (as revealed by the constancy of the corresponding $r_0(t_0)$), and double pore conductances were fit by the matching double pore candidate profiles. Interestingly from these examples, double pore cylindrical and conical-cylindrical profiles did a reasonable job of fitting single pore hyperbolic and double-conical conductance data, and single hyperbolic and double-conical candidates did a reasonable job of fitting double pore cylindrical and conical-cylindrical conductance data. Exact agreement still only occurs for correct shape and pore number, but the wrong profile doesn't inherently produce a terribly inaccurate radius. While they returned the incorrect shapes, the nevertheless fairly accurate r_0 means the expectations of which sizes of molecules would fit through the candidate pores are unlikely to differ appreciably, although the double pore case would allow for twice the number of channels and have different analyte-induced current blockages. Sufficient attention should therefore be obtained to optimizing the nanopore fabrication conditions,[40] and more involved post-fabrication characterizations should be considered if analyte-induced blockages do not fall within the range expected for the relative sizes of analyte and pore.[15, 16, 44, 45]

4 CONCLUDING REMARKS:

The performance of a nanopore used for applications such as single-molecule sensing, separations, and manipulations is dictated in large part by its size, shape, and surface chemistry. These three parameter groupings underpin the nanopore conductance, and allow a suitable analysis framework to use straightforward measurements of the conductance as a means to gain insight into these nanopore properties. Nanopore conductance is routinely used to coarsely gauge nanopore size during use, typically with at least the assumption of a cylindrical shape, and then often with deliberately incorrect parameter constraints to ensure that reasonable numerical estimates of the radius are nevertheless produced. More sophisticated conductance formalisms have been developed and validated for use with more complicated nanopore shapes and to account for additional considerations such as access resistance. Simple, analytical expressions allow for wider adoption of a characterization method that can easily accommodate a range of nanopore profiles, thereby providing both application flexibility and the possibility for using different model assumptions to explore the uncertainties in the extracted nanopore dimensions.[15, 16] New solution-based nanopore fabrication techniques have increased the importance of methods to characterize nanopores from their conductance. We tested the ability of a recently-developed method to characterize nanopores in real-time during fabrication by allowing for the possible formation of multiple pores or pores with defects. The simulations determined the correct nanopore number, size, and shape alongside the presence and size of any defects, but the numerical examples revealed challenges that await experimental applications of the approach. While the basic equations showed good agreement with experimental time-dependent conductance measurements, example characterizations that explicitly considered the possibility of nanofabrication defects yielded only very slight differences in the key metrics designed to identify nanopore profiles and

determine their dimensions. Inadequate measurement statistics may therefore impede the ability to uniquely or correctly determine the correct nanopore shape, number, and size. In challenging cases, a selection of analyses using different assumptions could produce a set of parameter values whose spread could offer a measure of the uncertainty of the characterization. Such real-time estimates could be followed by post-fabrication characterizations where larger conductance changes than those accompanying nanoscale changes of nanopore dimension would be wrought by changes of solution concentration, thereby easing the conductance analysis.[16] Thus, in spite of the limitations discussed here, the time-dependence of the nanopore conductance during fabrication remains a useful tool, given sufficient circumspection in application, for gaining insight into the evolving nanopore structure and for characterizing nanopores even without the usual assumptions of ideal formation.

Acknowledgements

This research has been supported by NSF CAREER award CBET-1150085, and by the University of Rhode Island, including URI graduate fellowships for Y. M. Nuwan D. Y. Bandara and Buddini Iroshika Karawdeniya. We thank Prof. Michael L. Greenfield for a considered reading of an earlier version of this manuscript, and the anonymous reviewer who proffered a scaling argument approach for the access resistance determination.

All authors declare no financial/commercial conflicts of interest.

5 REFERENCES

[1] Haywood, D. G., Saha-Shah, A., Baker, L. A., Jacobson, S. C., *Anal. Chem.* 2015, *87*, 172-187.
[2] Taniguchi, M., *Anal. Chem.* 2015, *87*, 188-199.
[3] Reiner, J. E., Balijepalli, A., Robertson, J. W. F., Campbell, J., Suehle, J., Kasianowicz, J. J., *Chem. Rev.* 2012, *112*, 6431-6451.
[4] Howorka, S., Siwy, Z., *Chem. Soc. Rev.* 2009, *38*, 2360-2384.
[5] Miles, B. N., Ivanov, A. P., Wilson, K. A., Dogan, F., Japrung, D., Edel, J. B., *Chem. Soc. Rev.* 2013, *42*, 15-28.

[6] Kudr, J., Skalickova, S., Nejdl, L., Moulick, A., Ruttkay–Nedecky, B., Adam, V., Kizek, R., *ELECTROPHORESIS* 2015, *36*, 2367-2379.
[7] Oukhaled, A., Bacri, L., Pastoriza-Gallego, M., Betton, J.-M., Pelta, J., *ACS Chemical Biology* 2012, *7*, 1935-1949.
[8] Branton, D., Deamer, D. W., Marziali, A., Bayley, H., Benner, S. A., Butler, T., Di Ventra, M., Garaj, S., Hibbs, A., Huang, X. H., Jovanovich, S. B., Krstic, P. S., Lindsay, S., Ling, X. S. S., Mastrangelo, C. H., Meller, A., Oliver, J. S., Pershin, Y. V., Ramsey, J. M., Riehn, R., Soni, G. V., Tabard-Cossa, V., Wanunu, M., Wiggin, M., Schloss, J. A., *Nat. Biotechnol.* 2008, *26*, 1146-1153.
[9] Sexton, L. T., Horne, L. P., Martin, C. R., *Molecular BioSystems* 2007, *3*, 667-685.
[10] Bayley, H., Martin, C. R., *Chem. Rev.* 2000, *100*, 2575-2594.
[11] Dwyer, J. R., Bandara, Y. M. N. D. Y., Whelan, J. C., Karawdeniya, B. I., Nichols, J. W., in: Edel, J., Ivanov, A., Kim, M. (Eds.), *Nanofluidics, 2nd Edition*, Royal Society for Chemistry 2016.
[12] Guo, P., Martin, C. R., Zhao, Y., Ge, J., Zare, R. N., *Nano Lett.* 2010, *10*, 2202-2206.
[13] Kowalczyk, S. W., Grosberg, A. Y., Rabin, Y., Dekker, C., *Nanotechnology* 2011, *22*, 315101.
[14] Bandara, Y. M. N. D. Y., Karawdeniya, B. I., Dwyer, J. R., *ACS Appl. Mater. Interfaces* 2016, *8*, 30583-30589.
[15] Frament, C. M., Bandara, N., Dwyer, J. R., *ACS Appl. Mater. Interfaces* 2013, *5*, 9330-9337.
[16] Frament, C. M., Dwyer, J. R., *J. Phys. Chem. C* 2012, *116*, 23315-23321.
[17] Smeets, R. M. M., Keyser, U. F., Krapf, D., Wu, M.-Y., Dekker, N. H., Dekker, C., *Nano Lett.* 2006, *6*, 89-95.
[18] Liebes, Y., Drozdov, M., Avital, Y. Y., Kauffmann, Y., Rapaport, H., Kaplan, W. D., Ashkenasy, N., *Appl. Phys. Lett.* 2010, *97*, 223105.
[19] Harms, Z. D., Haywood, D. G., Kneller, A. R., Jacobson, S. C., *Analyst* 2015, *140*, 4779-4791.
[20] Ayub, M., Ivanov, A., Instuli, E., Cecchini, M., Chansin, G., McGilvery, C., Hong, J., Baldwin, G., McComb, D., Edel, J. B., Albrecht, T., *Electrochim. Acta* 2010, *55*, 8237-8243.
[21] Stein, D., Kruithof, M., Dekker, C., *Phys. Rev. Lett.* 2004, *93*, 035901.
[22] Behrens, S. H., Grier, D. G., *J. Chem. Phys.* 2001, *115*, 6716-6721.
[23] DeBlois, R. W., Bean, C. P., *Rev. Sci. Instrum.* 1970, *41*, 909-916.
[24] Lee, C., Joly, L., Siria, A., Biance, A.-L., Fulcrand, R., Bocquet, L., *Nano Lett.* 2012, *12*, 4037-4044.
[25] Wanunu, M., Sutin, J., McNally, B., Chow, A., Meller, A., *Biophys. J.* 2008, *95*, 4716-4725.
[26] Aksimentiev, A., *Nanoscale* 2010, *2*, 468-483.
[27] Schoch, R. B., Han, J., Renaud, P., *Reviews of Modern Physics* 2008, *80*, 839-883.
[28] Vlassiouk, I., Smirnov, S., Siwy, Z., *Nano Lett.* 2008, *8*, 1978-1985.
[29] Anmiv, S. P., Talukder Zaki, N. J., Kevin, J. F., Rafael, M., Prashanta, D., Min Jun, K., *J. Phys.: Condens. Matter* 2010, *22*, 454107.
[30] Maglia, G., Restrepo, M. R., Mikhailova, E., Bayley, H., *Proceedings of the National Academy of Sciences* 2008, *105*, 19720-19725.
[31] Wolfe, A. J., Mohammad, M. M., Cheley, S., Bayley, H., Movileanu, L., *J. Am. Chem. Soc.* 2007, *129*, 14034-14041.
[32] Qiu, Y., Hinkle, P., Yang, C., Bakker, H. E., Schiel, M., Wang, H., Melnikov, D., Gracheva, M., Toimil-Molares, M. E., Imhof, A., Siwy, Z. S., *ACS Nano* 2015, *9*, 4390-4397.
[33] Yang, J., Ferranti, D. C., Stern, L. A., Sanford, C. A., Huang, J., Ren, Z., Qin, L.-C., Hall, A. R., *Nanotechnology* 2011, *22*, 285310.
[34] Li, J., Stein, D., McMullan, C., Branton, D., Aziz, M. J., Golovchenko, J. A., *Nature* 2001, *412*, 166-169.
[35] Storm, A. J., Chen, J. H., Ling, X. S., Zandbergen, H. W., Dekker, C., *Nature Materials* 2003, *2*, 537-540.
[36] Spinney, P. S., Howitt, D. G., Smith, R. L., Collins, S. D., *Nanotechnology* 2010, *21*, 375301.

[37] Vlassiouk, I., Apel, P. Y., Dmitriev, S. N., Healy, K., Siwy, Z. S., *Proceedings of the National Academy of Sciences of the United States of America* 2009, *106*, 21039-21044.
[38] Kwok, H., Briggs, K., Tabard-Cossa, V., *PLoS ONE* 2014, *9*, e92880.
[39] Whelan, J. C., Karawdeniya, B. I., Bandara, Y. M. N. D. Y., Velleco, B. D., Masterson, C. M., Dwyer, J. R., *ACS Appl. Mater. Interfaces* 2014, *6*, 10952-10957.
[40] Goto, Y., Yanagi, I., Matsui, K., Yokoi, T., Takeda, K.-i., *Scientific Reports* 2016, *6*, 31324.
[41] Williams, K. R., Muller, R. S., *J. Microelectromech. Syst.* 1996, *5*, 256-269.
[42] Kim, M. J., McNally, B., Murata, K., Meller, A., *Nanotechnology* 2007, *18*.
[43] Yanagi, I., Akahori, R., Hatano, T., Takeda, K.-i., *Sci. Rep.* 2014, *4*.
[44] Vogel, R., Willmott, G., Kozak, D., Roberts, G. S., Anderson, W., Groenewegen, L., Glossop, B., Barnett, A., Turner, A., Trau, M., *Anal. Chem.* 2011, *83*, 3499-3506.
[45] Nablo, B. J., Halverson, K. M., Robertson, J. W. F., Nguyen, T. L., Panchal, R. G., Gussio, R., Bavari, S., Krasilnikov, O. V., Kasianowicz, J. J., *Biophys. J.* 2008, *95*, 1157-1164.
[46] Makra, I., Jágerszki, G., Bitter, I., Gyurcsányi, R. E., *Electrochim. Acta* 2012, *73*, 70-77.

Figure Captions

Figure 1. a) Top view of $L(t_0) = 10$ nm cylindrical nanopores that yield a 200 nS conductance with the radii of the two inward-pointing defects given in the legend. b) Top view of the initially 1 nm-radius defect nanopore from (a), closing at $v_{\mathrm{mt}} = 0.6$ nm/h with deposition time indicated. c) Progression of conductance (and r_0^{pinch} in inset) with time for the cylindrical nanopores from (a).

Figure 2. (a) Experimental post-fabrication measurements of nanopore conductance and their corresponding TEM-based mean $r_{0,\mathrm{TEM}}^{\mathrm{expt}}$ (green stars)[43] were plotted versus several models: Equation 1 (solid markers) – cylindrical (red circles), double-conical (blue triangles), conical-cylindrical with an inner cylinder length of $0.6L$ (black squares), and hyperbolic (magenta diamonds); and with an added access resistance term, by Equation S1 (hollow markers) – cylindrical with length L (small circles) and cylindrical with a $0.37L$ effective length [43] (large circles). To not bias further analysis with an explicit choice of nanopore profile, the $r_{0,\mathrm{TEM}}^{\mathrm{expt}}$ were fit to Equation S1 with G_{bulk} and G_{surface} from the cylindrical model weighted by fit parameters: αG_{bulk} and $\beta G_{\mathrm{surface}}$ (orange triangles—$r_{0,\mathrm{TEM}}^{\alpha,\beta}(G)$). (b) Time-dependent conductance measurements were taken from the experimental work of Yanagi *et al.*[43] and were used with $r_{0,\mathrm{TEM}}^{\alpha,\beta}(G)$ to determine $r_{0,\mathrm{TEM}}^{\alpha,\beta}(t_i)$. (c) Candidate profiles matching those in (a) were used at each discrete value of $G(t_i)$ to calculate an $r_{0,\mathrm{candidate}}(t_i)$. The figure compares the fit and experimentally-derived radii where the correct candidate size should result in a straight line at a ratio of 1. Selected data markers are shown for clarity.

Figure 3. Conductances during simulated material deposition onto nanopores with initial conductances of 200 nS, and $r_0^{\mathrm{pinch}}(t_0) = 4$ nm, were fit with candidate cylindrical nanopores: a

defect-free pore, and pores with 0.1 and 1.0 nm-radius defects. Dotted and solid lines denote the pinch and outline radii, respectively. a) 0.1 nm defect pore and b) 1.0 nm defect pore profiles were used to furnish the simulated conductance data. The correct candidate profile in each case was indicated by the horizontal slope of the fit data; the defect-free $r_0(t_0)$ nearly completely overlaps with $r_0^{\text{pinch}}(t_0)$ for the 0.1 nm defect pores. Selected data markers are shown for clarity.

Figure 4. a) Conductances and (inset) radii as a function of profile and time when simulating deposition onto surfaces of initially 200 nS, $L(t_0) = 10$ nm nanopores. Dotted curves in the conductance plots belong to the cylindrical pores with defects, and denote the corresponding r_0^{pinch} in the inset (solid line-r_0^{outline}) and in (b)-(c).Conductance versus time for b) 0.1 nm-defect and c) 1.0 nm-defect cylindrical pores were fit with each candidate profile in the legend; horizontal fit lines for each case indicated the correct simulated profile. Selected data markers are shown for clarity.

Figure 5. Single (solid lines) and double (dotted lines)—left to right matching the half-profile sketches—cylindrical (red circles), double-conical (blue triangles), conical-cylindrical (black squares), and hyperbolic (magenta diamonds) profiles were used to simulate nanopore conductance values versus time. Eight candidate profiles (4 shapes, single and double) were used to fit (a-d) single pore simulated data and (e-h) double pore data from the 4 shapes. All experimental pores were initially 200 nS conductance. The correct nanopore shape was indicated by the constancy of the fit to $r_0(t_0)$ in time, and is labelled with the corresponding shape and number of pores. Selected data markers are shown for clarity.

Figure 1

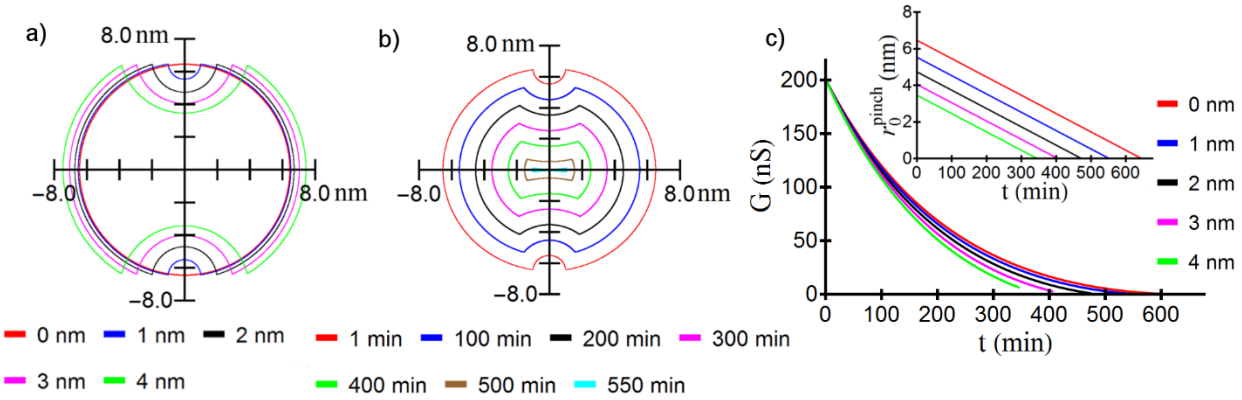

Figure 2

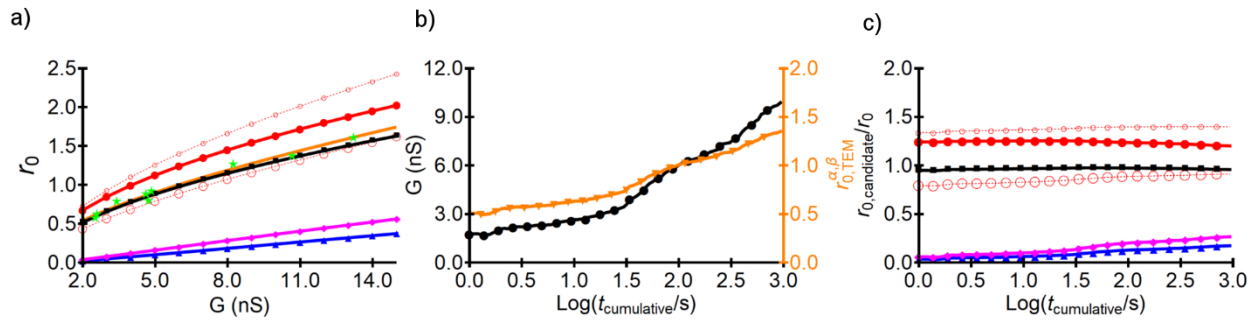

Figure 3

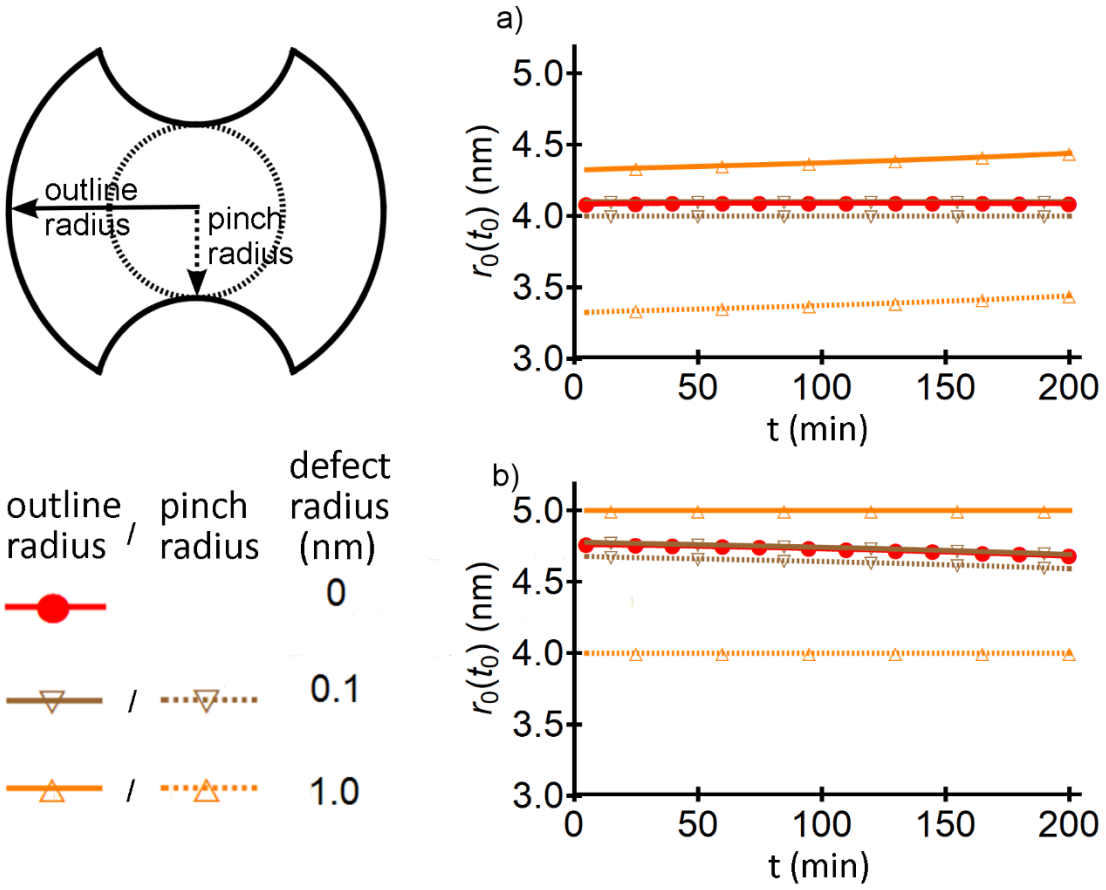
outline radius
pinch radius
a)
b)
$r_0(t_0)$ (nm)
t (min)
5.0
4.5
4.0
3.5
3.0
0
50
100
150
200
outline radius / pinch radius
defect radius (nm)
0
0.1
1.0

Figure 4

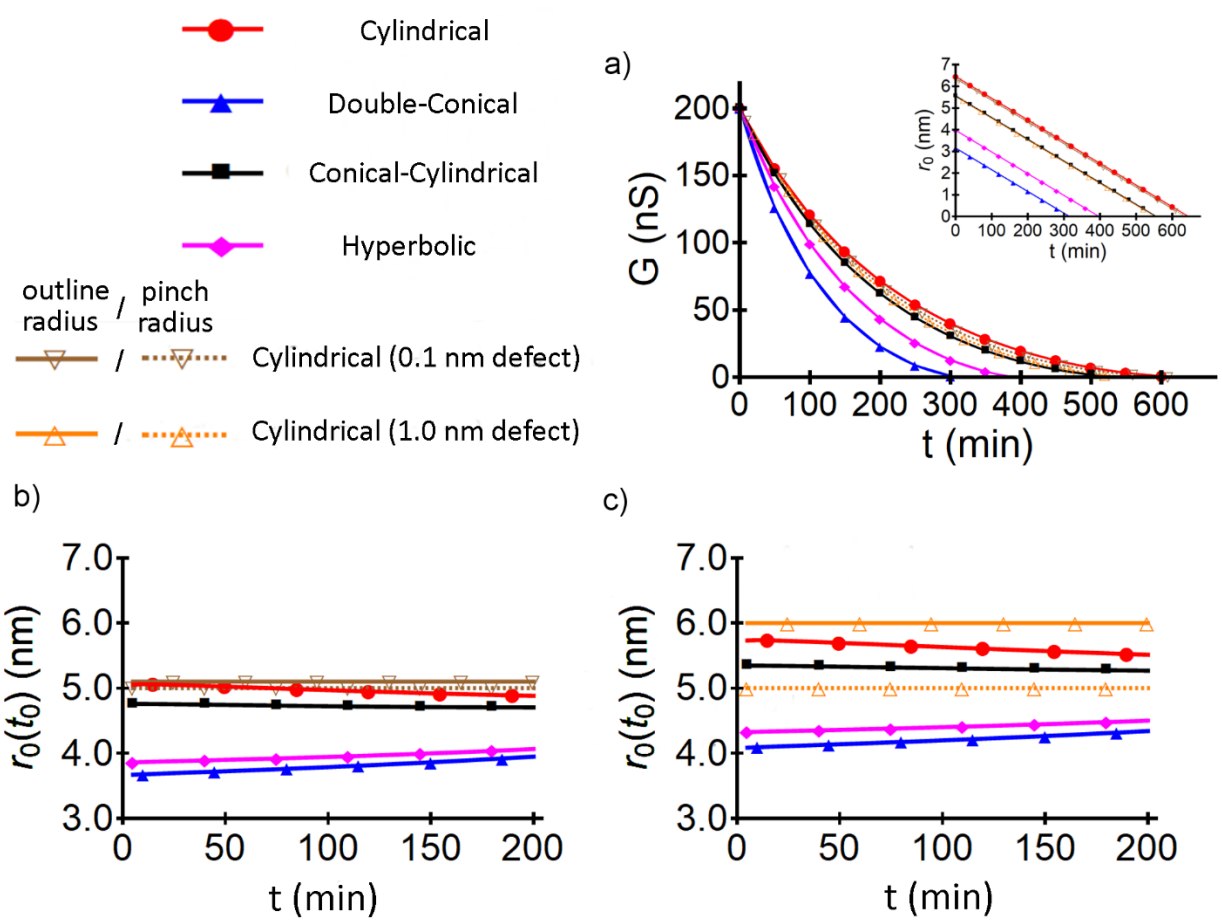
Cylindrical
Double-Conical
Conical-Cylindrical
Hyperbolic
outline radius / pinch radius
Cylindrical (0.1 nm defect)
Cylindrical (1.0 nm defect)
a)
G (nS)
t (min)
r_0 (nm)
b)
c)
$r_0(t_0)$ (nm)
t (min)

Figure 5

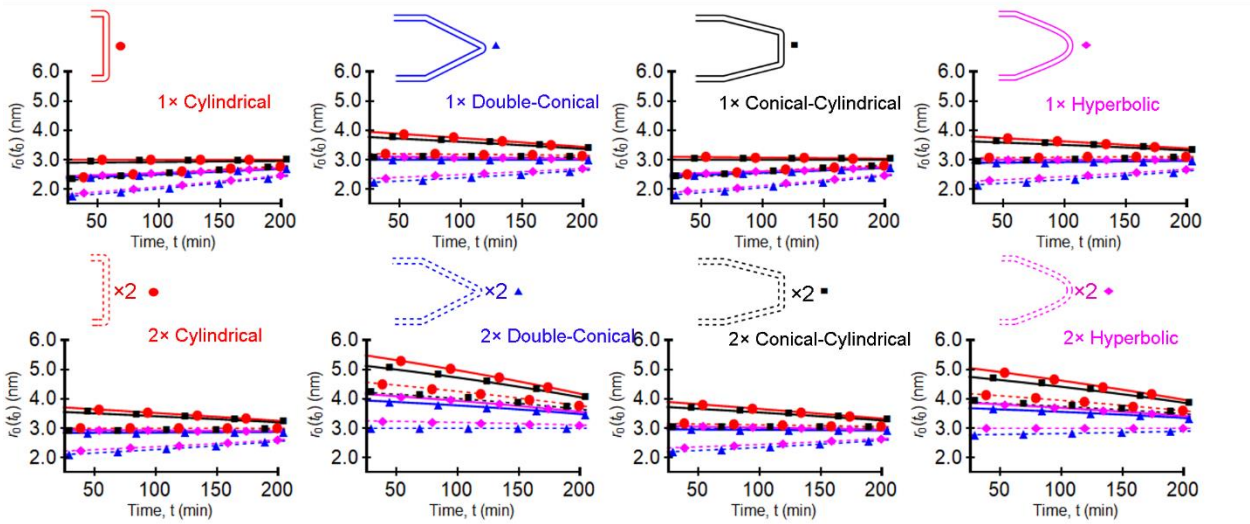
1× Cylindrical
1× Double-Conical
1× Conical-Cylindrical
1× Hyperbolic
2× Cylindrical
2× Double-Conical
2× Conical-Cylindrical
2× Hyperbolic
×2
$r_0(t_0)$ (nm)
Time, t (min)